

MULTI-WAVELENGTH AFTERGLOWS IN GAMMA-RAY BURSTS: REFRESHED SHOCK AND JET EFFECTS

A. Panaiteescu, P. Mészáros

Department of Astronomy & Astrophysics, Pennsylvania State University, University Park, PA 16802

and

M. J. Rees

Institute of Astronomy, University of Cambridge, Madingley Road, Cambridge, CB3 0HA, U.K.

ABSTRACT

We present an analytical approach to calculate the hydrodynamics of the interaction between a relativistic ejecta and a surrounding medium, whose evolution serves as a model for Gamma-Ray Burst afterglows. We investigate the effect of the relevant model parameters on the X-ray, optical and radio fluxes, and the effect of a refreshed shock energy input and anisotropy in the ejecta on the shape of the light-curves. We compare our numerical results to observed afterglows and give a quantitative description of the conditions (geometry and physical parameters) in the ejecta that are compatible with the light-curves of the 970508 afterglow, for which a large number of accurate flux measurements are available. We find that the radio, optical and X-ray light-curves of this afterglow can be explained satisfactorily within the spherically symmetric fireball model, assuming a delayed energy injection, or by an axially symmetric jet surrounded by a less energetic outflow.

Subject headings: gamma-rays: bursts - methods: numerical - radiation mechanisms: non-thermal

1. Introduction

Afterglows from Gamma-Ray Bursts (GRBs) have been observed from a number of objects at X-ray, optical, and in one case also at radio wavelengths. Simple analytical models are successful at explaining the major features of the light-curves (Mészáros & Rees 1997, Vietri 1997, Tavani 1997, Waxman 1997; Wijers, Rees & Mészáros 1997). The optical and X-ray light curves presented by many authors (e.g. Pedersen et al. 1998, Piro et al. 1998, Garcia et al. 1998, Bartolini et al. 1998) have provided evidence for occasional departures from the basic overall power-law decay behavior. Such departures, as well as the possibility of temporal power-law decays that are not exclusively determined by the spectral index, have been shown to follow naturally from fireball models where the radiative regime changes, the energy is not distributed isotropically in the ejecta (Mészáros, Rees & Wijers 1998), or where the energy input depends on the Lorentz factor during the brief injection episode of the central engine, leading to refreshed shocks (Rees & Mészáros 1998). Here we go beyond simple analytical asymptotic models, we derive and solve numerically the differential equations for the dynamics of the afterglow in the general case of a inhomogeneous external medium and refreshed shock mechanism, and calculate numerically the light-curves arising in such scenarios.

Our previous numerical work (Panaiteescu & Mészáros 1997, 1998) on simulations of light-curves and spectra was based on a hydrodynamic code (Wen, Panaiteescu & Laguna 1997) that solves the equations of relativistic hydrodynamics and the shock jump conditions. The energy release mechanisms (synchrotron

and inverse Compton) were treated as described in Panaiteescu & Mészáros (1997). A calculation of the spectra and time history of an afterglow from a spherically symmetric shocked fireball is equivalent to computing a quadruple integral: over the lab frame time, over the structure of the shocked fluid, over the angle relative to the line of sight toward the fireball center (LSC) of symmetry and over the electron distribution. The hydrodynamic timesteps required to propagate the shell of shocked fluid over times that are more than 5 orders of magnitude larger than the shell crossing time and those necessary for an accurate calculation of the radiative losses lead to exceedingly long numerical runs, which are not best suited for an investigation of the effects of the large number of model parameters involved in the typical external shock scenario of GRBs and afterglows (Mészáros & Rees 1997). The numerical task is even more time-consuming in the case of anisotropic ejecta, where a new integral over the azimuthal angle is added.

To acquire computational speed, we have developed a numerical code that calculates accurately the evolution of the remnant shell's flow Lorentz factor, by solving the equation that gives the evolution of the kinetic energy of the remnant during the ejecta–external medium interaction, with allowance for an energy injection in the reverse shock (Rees & Mészáros 1998), and radiative and adiabatic losses. Anisotropy of the ejecta or of the energy input is included at the simplest level, assuming cylindrical symmetry around an axis that is not necessarily the same as the LSC. Despite the assumed degree of symmetry in the ejecta, the resulting light-curves show a great diversity. Possible inhomogeneity of the external medium is considered in the form of a power-law density. To simplify the energy release treatment, we ignore here the inverse Compton scattering of the self-generated synchrotron photons, which is a fairly good assumption, substantiated by our previous results (Panaiteescu & Mészáros 1998). In what follows we describe the analytic treatment of the remnant's dynamics and energetics, derive analytic light-curves and present our numerical results. We discuss the effect of model parameters on the features of the numerical light-curves, and compare them with the afterglow of GRB 970508.

2. Hydrodynamics of the Remnant and Energy Release

The most important parameter characterizing the temporal evolution of the afterglow is the bulk Lorentz factor Γ of the contact discontinuity between the ejecta and the swept up external matter. The evolution of Γ is determined by two main factors, the hydrodynamics of the shell (including the energy input, adiabatic losses and the deceleration caused by the external medium) and the radiative losses (synchrotron cooling).

2.1. Adiabatic remnant

In the absence of a delayed energy injection and of radiative losses (adiabatic remnant), at any time, the total energy of the fireball is constant: $d[M(\Gamma - 1) + \Gamma U] = 0$, where $M = M_0 + M_{ex}$ is the total remnant mass (the sum of the initial ejecta mass M_0 and the swept-up mass M_{ex}) and U is the co-moving frame internal energy of the remnant. The evolution of U is given by the adiabatic losses and by the heating of the external matter: $dU = (dU)_{ad} + (dU)_{ex}$. The jump conditions (Blandford & McKee 1976) at the forward shock imply that $(dU)_{ex} = (\Gamma - 1) dM_{ex} c^2$, where c is the speed of light, therefore the energy conservation can be written as:

$$(Mc^2 + U) d\Gamma + \Gamma (dU)_{ad} + (\Gamma^2 - 1) dM_{ex} c^2 = 0, \quad (1)$$

where $dM_{ex} = 4\pi r^2 \rho_{ex}(r) dr$ and $(dU)_{ad} = -(\hat{\gamma} - 1) U d(\ln V')_{ad}$. The first term in equation (1) is the lab-frame change in the kinetic energy, the second represents the adiabatic losses and the third is the total

lab-frame kinetic energy of the shocked external medium, including its internal energy. In the above equations r is the radial coordinate of the thin remnant, $\rho_{ex} = \rho_d(r/r_d)^{-\alpha}$, ρ_d is the external medium density at the deceleration radius r_d , defined as the radius where the swept up mass is a fraction Γ_0^{-1} of the initial fireball mass M_0 , Γ_0 being its initial Lorentz factor, $\alpha < 3$ is the index of the external matter power-law density, $\hat{\gamma}$ is the adiabatic index (maintained close to 4/3 even when $\Gamma \lesssim 2$ by the relativistic electrons, provided that the fraction of electrons that are shock-accelerated is not too much below unity) and V' is the remnant comoving volume. The differential $d(\ln V')_{ad}$ refers to that part of the comoving volume that is occupied by the already shocked fluid, i.e. it excludes the change in the comoving volume due to the sweeping up of the infinitesimal dM_{ex} .

We assume that the shocked external fluid stores most of the internal energy of the remnant and that it gives most of the afterglow radiation, as the forward shock is more relativistic than the quasi-newtonian reverse shock, and thus more efficient in converting kinetic energy into internal and in accelerating high energy electrons that are less adiabatic than the electrons accelerated by the reverse shock. Therefore, in this work we neglect the dynamical and radiative importance of the reverse shock, and leave its treatment for a future, more detailed study. We also assume that the remnant volume is practically given by the volume of the shocked external medium (which is correct if the injected mass is not too large compared to the mass of swept up external medium, because the ejecta compressed between the contact discontinuity and the reverse shock is denser than the shocked external medium) and that the comoving density behind the blast wave is equal to that set by the shock jump conditions. This implies that the comoving density is determined solely by $\rho_{ex}(r)$ and Γ : $\rho'(r) = (\hat{\gamma} + 1)^{-1}(\hat{\gamma}\Gamma + 1)\rho_{ex}(r)$. Using $d(\ln V')_{ad} = -d(\ln \rho')$, the adiabatic losses can be written as:

$$(dU)_{ad} = -(\hat{\gamma} - 1) \left(\frac{\alpha}{r} - \frac{\hat{\gamma}}{\hat{\gamma}\Gamma + 1} \frac{d\Gamma}{dr} \right) U dr. \quad (2)$$

The shocked external medium mass is given by

$$dM_{ex} = 3 \frac{M_0}{\Gamma_0} \frac{r^{2-\alpha}}{r_d^{3-\alpha}} dr, \quad (3)$$

which allows one to calculate the comoving volume $V' = M_{ex}/\rho'$.

2.2. Delayed Energy Input

It is possible that the material injected by the cataclysmic event that generates the relativistic fireball does not have a unique Γ_0 , and that some material is ejected with lower initial bulk Lorentz factors, down to some limiting Γ_m . Following Rees & Mészáros (1998), we shall consider that all the ejecta has been released impulsively (on a timescale short compared to the afterglow timescale), all at the same location, and with a power-law distribution of energy per unit Lorentz factor Γ_f : $dE_f \propto \Gamma_f^{-s} d\Gamma_f$, for $\Gamma_m < \Gamma_f < \Gamma_d$, where $\Gamma_d < \Gamma_0$ is the Lorentz factor of the contact discontinuity at $r = r_d$ (for reasons given below, we start our simulations at $r = r_d$). The constant of proportionality is determined by the total injected energy E_{inj} , which will be one of the free parameters of the model. The fluid moving at lower Γ_f lags behind the contact discontinuity and catches up with it later, as the fireball is progressively decelerated by the interaction with the external fluid. From the kinematics of the problem, the Lorentz factor of the ejecta that interacts with the reverse shock at radius r is given by

$$d\Gamma_f = -\frac{\Gamma_f}{2} \left[(\Gamma_f/\Gamma)^2 - 1 \right] \frac{dr}{r}. \quad (4)$$

The mass injected in the remnant up to radius r satisfies the differential equation

$$dM_f = F_s(\Gamma_f, \Gamma) M_{inj} \frac{dr}{r}, \quad (5)$$

where

$$F_s(\Gamma_f, \Gamma) = \frac{s}{2} \frac{(\Gamma_f/\Gamma)^2 - 1}{1 - (\Gamma_m/\Gamma_d)^s} \left(\frac{\Gamma_m}{\Gamma_f} \right)^s. \quad (6)$$

Here M_{inj} is the total mass that is eventually injected in the remnant, which corresponds to an E_{inj} given by

$$E_{inj} = \frac{s(s-1)^{-1} [1 - (\Gamma_m/\Gamma_d)^{s-1}] \Gamma_m + (\Gamma_m/\Gamma_d)^s - 1}{1 - (\Gamma_m/\Gamma_d)^s} M_{inj} c^2. \quad (7)$$

As the shocked shell propagates from r to $r + dr$, the infinitesimal injected mass dM_f given by equation (5) collides with the shell, increasing the remnant kinetic energy by $dE_{k,f}$ and its internal energy by $(dU)_f$. These infinitesimal energies can be determined from momentum and energy conservation:

$$dE_{k,f} = \Gamma_f [1 - \Gamma^2(1 - \beta\beta_f)] dM_f c^2, \quad (8)$$

$$(dU)_f = [\Gamma\Gamma_f(1 - \beta\beta_f) - 1] dM_f c^2, \quad (9)$$

where β represents the velocity in units of c .

2.3. Radiative Losses

As mentioned before, we consider here that the shocked fluid cools through adiabatic expansion and emission of synchrotron radiation from electrons accelerated by the forward shock. There could be some contribution to the early afterglow light-curve from electrons accelerated by the reverse shock, but this is soon overcome by the forward shock emission that shifts toward lower energies, as the remnant is decelerated. We assume that nearly all electrons are shock-accelerated to a power-law distribution of index $p > 1$, $dn'_e \propto \gamma_e^{-p} d\gamma_e$, for $\gamma_m < \gamma_e < \gamma_M$, where n'_e is the co-moving electron number density, γ_e is the electron random Lorentz factor, and we ignore a possible tail of thermal electrons with $\gamma_e < \gamma_m$. The maximum γ_M is determined by the synchrotron losses during the acceleration timescale, and, for most of the afterglow, is several orders of magnitude larger than γ_m . The minimum γ_m is set by parameterizing the total energy density stored in electrons after acceleration, as a fraction ε_{el} of the internal energy density of the shocked fluid (which is given by the jump conditions at shock – Blandford & McKee 1976), and by the injection fraction ζ of electrons that are accelerated at shock. The result is

$$\gamma_m = \frac{p-2}{p-1} \frac{1 - (\gamma_M/\gamma_m)^{1-p}}{1 - (\gamma_M/\gamma_m)^{2-p}} \left[1 + \frac{\varepsilon_{el}}{\zeta} \frac{m_p}{m_e} (\Gamma - 1) \right]^{p>2} \frac{\varepsilon_{el}}{\zeta} \frac{p-2}{p-1} \frac{m_p}{m_e} (\Gamma - 1), \quad (10)$$

m_p and m_e being the proton and electron masses, respectively.

The comoving magnetic field B is assumed to be turbulent and is parameterized through the fraction ε_{mag} of the internal energy that is in the form of magnetic field energy,

$$B = \sqrt{8\pi \varepsilon_{mag} \frac{U}{V'}} = B_0 \left[\varepsilon_{mag} \frac{\hat{\gamma}\Gamma + 1}{\hat{\gamma} - 1} \frac{3 - \alpha}{3a^3 - \alpha a^\alpha} u \right]^{1/2}, \quad (11)$$

where $B_0 = (8\pi\Gamma_0\rho_dc^2)^{1/2} = 1.94(n_0\Gamma_{0,2})^{1/2}$ G, n_0 being the external medium particle density at the deceleration radius, in cm^{-3} , $\Gamma_{0,2} = 10^{-2}\Gamma_0$ and the non-dimensional variables $a = r/r_d$ and $u = U/M_0c^2$ have been used.

The radiative losses are given by a double integral over the remnant volume and the electron distribution,

$$(dU)_{rad} = - \int dV' \int_{\gamma_m(t')}^{\gamma_M(t')} dn'_e(\gamma_e) P'_{sy}(\gamma_e) dt' , \quad (12)$$

which can be calculated for given B and $dn'_e(\gamma_e)$ at each point in the shocked structure. In equation (12), $P'_{sy}(\gamma_e) = (4/3)\sigma_{Th}c(B^2/8\pi)(\gamma_e^2 - 1)$ is the synchrotron power (σ_{Th} being the cross-section for electron scattering) and $dt' = (\Gamma^2 - 1)^{-1/2}c^{-1}dr$ gives the comoving frame time. The electron distribution in each infinitesimal “sub-shell” within the volume of the shocked fluid is calculated by first initializing it at the time t' when the sub-shell is added to the shocked structure and then tracking the evolution of the electron Lorentz factor γ_e , subject to adiabatic and radiative losses:

$$\frac{d\gamma_e}{da} = -\frac{1}{3} \frac{d\ln V'}{da} (\gamma_e - 1) - \frac{1}{6\pi} \frac{\sigma_{Th}B^2}{m_e c} \frac{dt'}{da} (\gamma_e^2 - 1) . \quad (13)$$

2.4. Differential Equations and Initial Conditions

We can now add the contribution of the material injection at the reverse shock given by equation (8) to the evolution of Γ (eq. [1]), and obtain:

$$\frac{d\Gamma}{da} = \frac{\Gamma_f[1 - \Gamma^2(1 - \beta\beta_f)]F_s(\Gamma_f, \Gamma)\omega_M + (\hat{\gamma} - 1)\alpha\Gamma u - 3(\Gamma^2 - 1)\Gamma_0^{-1}a^{3-\alpha}}{a[\mu + (\hat{\gamma}^2\Gamma + 1)(\hat{\gamma}\Gamma + 1)^{-1}u]} , \quad (14)$$

where $\mu = M/M_0$ is the dimensionless remnant mass and $\omega_M = M_{inj}/M_0$ is the dimensionless total injected mass. We can also obtain the differential equation for U by including the internal energy input (eq. [9]) and the radiative losses (eq. [12]):

$$\frac{du}{da} = [\Gamma_f\Gamma(1 - \beta\beta_f) - 1]F_s(\Gamma_f, \Gamma)\frac{\omega_M}{a} - (\hat{\gamma} - 1)\left(\frac{\alpha}{a} - \frac{\hat{\gamma}}{\hat{\gamma}\Gamma + 1}\frac{d\Gamma}{da}\right)u + 3a^{2-\alpha}\frac{\Gamma - 1}{\Gamma_0} + \left(\frac{du}{da}\right)_{rad} . \quad (15)$$

The first term in the numerator of equation (14) and the first term in the right hand side of equation (15) are switched off when Γ_f , calculated by integrating equation (4), drops below Γ_m . The differential equation for the mass of the remnant can be obtained with the aid of equations (3) and (5):

$$\frac{d\mu}{da} = \frac{3a^{2-\alpha}}{\Gamma_0} + F_s(\Gamma_f, \Gamma)\frac{\omega_M}{a} . \quad (16)$$

Solving the hydrodynamics of the remnant is therefore equivalent to integrating the set of coupled differential equations (4), (14), (15) and (16). These equations are valid in any relativistic regime. If all the released ejecta has the same initial Lorentz factor, then the fireball is not entirely crossed by the the reverse shock if $r < r_d$ and the yet unshocked part of the ejecta and the shocked fluid move with different Lorentz factors. To avoid unnecessary complications, we simulate the dynamical evolution of the fireball starting from $r = r_d$ and pass over the $r < r_d$ stage by making an appropriate choice of the initial conditions at $r = r_d$. These initial conditions are determined by the definition of r_d . The energy released before r_d , can be safely neglected, so that, by equating the sum of the kinetic energy $(1 + \Gamma_0^{-1})(\Gamma_d - 1)M_0c^2$ and the lab frame

internal energy $\sim \Gamma_d(\Gamma_d - 1)(M_0/\Gamma_0)c^2$ at r_d with the initial energy $E_0 = (\Gamma_0 - 1)M_0c^2$, it is straightforward to show that $\Gamma_d = 0.62\Gamma_0$ and $U(r_d) = (\Gamma_d - 1)(M_0/\Gamma_0)c^2 \sim 0.62 M_0c^2$. Therefore the initial conditions are

$$\Gamma(a = 1) = \Gamma_f(a = 1) = 0.62\Gamma_0, \quad u(a = 1) = 0.62, \quad \text{and} \quad \mu(a = 1) = 1 + \Gamma_0^{-1}. \quad (17)$$

3. Analytical Asymptotic Light-Curves

The temporal history of the afterglow flux received at Earth can be calculated analytically by assuming that the ejecta is either spherically symmetric or is a jet with axial symmetry, and that Γ is power-law in r . The last assumption is correct only over a certain range of times; a different treatment is needed when the remnant slows down to non-relativistic speeds. We consider here relativistically expanding remnants and, for simplicity, in this section we neglect energy injection and restrict our attention to the case when the remnant is adiabatic, as it is most likely that this stage lasts the longest (Waxman, Kulkarni & Frail 1998). Electrons can be either radiative or adiabatic. The former case is compatible with the assumption of an adiabatic remnant provided that electrons are not re-energized after shock acceleration or that ε_{el} is small enough that most of the internal energy is stored in protons and magnetic fields and lost adiabatically. In what follows, we denote by γ_m the minimum Lorentz factor of the electrons (in the power-law distribution) that have just been accelerated, i.e. those electrons that are located very close the forward shock.

For a relativistic and adiabatic remnant, to a good approximation, the Lorentz factor of the contact discontinuity evolves as (Mészáros et al. 1998)

$$\Gamma \sim \Gamma_d(r/r_d)^{-(3-\alpha)/2}, \quad (18)$$

where we consider only the $\alpha < 3$ case. The definition of r_d gives $r_d \propto (E_0 n_d^{-1} \Gamma_0^{-2})^{1/3}$, where n_d is the external medium particle density at r_d , and where a multiplying factor that has a weak dependence on α has been ignored. For definiteness, we consider that the power-law behavior of the external medium density is manifested beyond a radius R_d , up to which the external density is almost constant, with R_d large enough to cover all the possible values of the deceleration radii encountered in fireballs with reasonable values of the parameters Γ_0 and E_0 . This approximation is not affecting the remnant evolution, as the afterglow radiation is emitted at radii much larger than R_d . Using the relationship between the observer time T and the lab-frame time t , $T \propto t/\Gamma^2$, the T -dependence of the Lorentz factor is found to be

$$\Gamma \propto \left[(E_0/n_d)^{(3-\alpha)/2} \Gamma_0^\alpha \right]^{1/(12-3\alpha)} T^{-(3-\alpha)/(8-2\alpha)}. \quad (19)$$

Note that Γ is independent on Γ_0 if the external medium is homogeneous. As seen by the observer, the (transverse) source size scales as ΓT if the ejecta is spherically symmetric. The received flux F_{ν_p} at the peak ν_p of the synchrotron spectrum is $F_{\nu_p} \propto (\Gamma T)^2 \Gamma^3 I'_{\nu'_p}$ (Mészáros et al. 1998), where $I'_{\nu'_p}$ is the comoving synchrotron intensity at the comoving peak frequency ν'_p .

Radiative Electrons. If electrons are radiative, then $I'_{\nu'_p} \propto n'_e (P'_{sy}/\nu'_p) t'_{sy} \propto n'_e (\gamma_m B)^{-1}$, where t'_{sy} is the comoving synchrotron cooling timescale and where we substituted $P'_{sy} t'_{sy} \propto \gamma_m$. The magnetic field can be calculated using equation (11), where the comoving internal energy is determined by assuming that the lab frame internal energy of the adiabatic remnant is a (constant) fraction of the initial energy: $\Gamma u \propto E_0 \implies B \propto \varepsilon_{mag}^{1/2} (n_d^{3-\alpha} \Gamma_0^{-2\alpha} E_0^\alpha)^{1/6} r^{-\alpha/2} \Gamma$. The same result can be obtained using the jump conditions at the forward shock: $B^2 \propto \varepsilon_{mag} (dU/dV') \propto \varepsilon_{mag} \rho' \Gamma \propto \varepsilon_{mag} \rho_{ex} \Gamma^2$. By using equations (10) (with $p > 2$), (19) and $r \propto \Gamma^2 T$, one can calculate $I'_{\nu'_p}$ and the evolution of the observed peak frequency $\nu_p \propto \gamma_m^2 B \Gamma$. If

observations are made at a frequency $\nu < \nu_p$, the observer “sees” the low energy tail of the synchrotron spectrum, which has a slope of $1/3$. Then $F_\nu = (\nu/\nu_p)^{1/3} F_{\nu_p}$, leading to

$$F_{rad}(\nu < \nu_p) \propto \varepsilon_{mag}^{-2/3} \varepsilon_{el}^{-5/3} \zeta^{8/3} E_0^{1/3} T. \quad (20)$$

Above ν_p , the synchrotron spectrum has a slope $-p/2$, yielding:

$$F_{rad}(\nu > \nu_p) \propto \varepsilon_{mag}^{(p-2)/4} \varepsilon_{el}^{p-1} \zeta^{2-p} E_0^{(p+2)/4} T^{-(3p-2)/4}. \quad (21)$$

Note that $F_{rad}(\nu)$ is independent on the external medium parameters (α, n_d) and on the fireball initial Lorentz factor and that it depends strongly (powers close to or above 1) on ε_{el} and also on ζ if $\nu < \nu_p$ and on E_0 if $\nu > \nu_p$.

Adiabatic Electrons. If the electrons are adiabatic, then $I'_{\nu_p} \propto n'_e (P'_{sy}/\nu'_p) \Delta' \propto n'_e B \Delta'$, where Δ' is the comoving remnant thickness. The product $n'_e \Delta'$ can be calculated using the fact that $4\pi (n'_e/\zeta) m_p r^2 \Delta'$ is the external medium mass swept up until radius r is reached. Below the spectral peak

$$F_{ad}(\nu < \nu_p) \propto \varepsilon_{mag}^{1/3} \varepsilon_{el}^{-2/3} \zeta^{5/3} \left[\Gamma_0^{-4\alpha} E_0^{2(5-\alpha)} n_d^{2(3-\alpha)} \right]^{1/(12-3\alpha)} T^{(2-\alpha)/(4-\alpha)}. \quad (22)$$

For observations made above ν_p , the synchrotron spectrum has a slope $-(p-1)/2$, therefore:

$$F_{ad}(\nu > \nu_p) \propto \varepsilon_{mag}^{(p+1)/4} \varepsilon_{el}^{p-1} \zeta^{2-p} \left[\Gamma_0^{-4\alpha} E_0^{3(p+3)-\alpha(3p+7)/4} n_d^{2(3-\alpha)} \right]^{1/(12-3\alpha)} T^{-[3(p-1)/4]-[\alpha/(8-2\alpha)]}. \quad (23)$$

Generally, the light-curve has a strong dependence on E_0 and ε_{el} , and also on ζ if $\nu < \nu_p$ and on ε_{mag} if $\nu > \nu_p$. Other dependences are weak to moderate. For $\alpha \gtrsim 2$, the light-curve depends strongly on Γ_0 and $F_{ad}(\nu < \nu_p)$ increases with T . The larger α , the faster $F_{ad}(\nu > \nu_p)$ decreases with T .

Jets. If the ejecta is jet-like (Waxman et al. 1998), then equations (20) – (23) give the correct observed flux in the early afterglow, when the observer does not see the edge of the jet or the effect of the sideways escape of the ejecta (Rhoads 1998). For an observer located at an angle θ_{obs} relative to the jet axis and a jet of half-angular opening θ_{jet} such that $\theta_{obs} \ll \theta_{jet}$, the jet edge is seen after Γ drops below θ_{jet}^{-1} . In this case, the source size is $\propto r \theta_{jet} \propto \Gamma^2 T \theta_{jet}$. The light-curve of the afterglow from a jet-like remnant is given by:

$$F_{rad}(\nu < \nu_p) \propto \varepsilon_{mag}^{-2/3} \varepsilon_{el}^{-5/3} \zeta^{8/3} \left[\Gamma_0^{2\alpha} E_0^{7-2\alpha} n_d^{-(3-\alpha)} \right]^{1/(12-3\alpha)} T^{1/(4-\alpha)}, \quad (24)$$

$$F_{rad}(\nu > \nu_p) \propto \varepsilon_{mag}^{(p-2)/4} \varepsilon_{el}^{p-1} \zeta^{2-p} \left[\Gamma_0^{2\alpha} E_0^{3(p+3)-\alpha(3p+10)/4} n_d^{-(3-\alpha)} \right]^{1/(12-3\alpha)} T^{-(3p/4)-[(2-\alpha)/(8-2\alpha)]}, \quad (25)$$

if electrons are radiative and by

$$F_{ad}(\nu < \nu_p) \propto \varepsilon_{mag}^{1/3} \varepsilon_{el}^{-2/3} \zeta^{5/3} \left[\Gamma_0^{-2\alpha} E_0^{13-3\alpha} n_d^{3-\alpha} \right]^{1/(12-3\alpha)} T^{-1/(4-\alpha)}, \quad (26)$$

$$F_{ad}(\nu > \nu_p) \propto \varepsilon_{mag}^{(p+1)/4} \varepsilon_{el}^{p-1} \zeta^{2-p} \left[\Gamma_0^{-2\alpha} E_0^{3(p+4)-\alpha(3p+11)/4} n_d^{3-\alpha} \right]^{1/(12-3\alpha)} T^{-[3(p-1)/4]-[(6-\alpha)/(8-2\alpha)]}, \quad (27)$$

if electrons are adiabatic.

A comparison of equations (20)-(23) and (24)-(27) shows that the light-curve from beamed ejecta rises slower and decays faster than that from a spherical fireball. At the onset of the $\Gamma < \theta_{jet}^{-1}$ phase, the decay of the afterglow steepens by $(3 - \alpha)/(4 - \alpha)$, yielding a break in the light-curve. This phase lasts until the escape of the ejecta outside the cone in which it was initially released becomes important. Rhoads (1998)

has shown that in this case the remnant bulk Lorentz factor decreases exponentially with radius, and that the decay of the afterglow light-curve exhibits another break, but remains a power-law in the observer time. It can be shown that the time interval from the onset of the exponential phase and the beginning of the non-relativistic phase is $2.3(\theta_{jet}/10^\circ)^2$ times shorter than the duration of the $\Gamma < \theta_{jet}^{-1}$ phase and that unless $\theta_{jet} \lesssim 7^\circ$ (which yields a very low probability of observing the afterglow) the sideways escape phase occurs after the remnant becomes non-relativistic.

Mixed Electron Radiative Regimes. Equations (20)–(27) were derived assuming that all the electrons are either radiative or adiabatic. The real situation is more complex, as the more energetic tail of the power-law distribution of electrons contains electrons that are radiative and contribute more to the received flux at some given frequency $\nu \gg \nu_p(\gamma_m)$ than the less energetic γ_m -electrons, which become adiabatic early in the afterglow. In fact this is the case with most of the numerical X-ray and optical afterglows shown in the next section. If the γ_m -electrons are adiabatic, the flux at a frequency where the emission is dominated by more energetic and radiative electrons can be derived using the $I'_{\nu'_p}$ calculated for adiabatic electrons and the fact that the spectrum has a slope $-(p-1)/2$ for frequencies above ν_p and below the peak frequency of the synchrotron emission from electrons that have a radiative timescale equal to the adiabatic one, and a slope $-p/2$ above this frequency. Interestingly, the result is the same as given by equations (21) and (25) for radiative γ_m -electrons, i.e. only the constants of proportionality are altered.

We should keep in mind that the above analytical derivations do not take into account the shape of the equal arrival time surface, i.e. the fact that photons that arrive simultaneously at detector were emitted at different lab-frame times. Moreover, we ignored the fact that there are electrons with Lorentz factors below the γ_m of the freshly accelerated electrons. For these reasons, the equations (20)–(27) are of somewhat limited use and, for more accurate results, one must integrate numerically the afterglow emission.

4. Numerical Results

We have introduced so far the following model parameters: (1) dynamical parameters $(E_0; n_d, \alpha; \Gamma_0)$, (2) late energy injection parameters (E_{inj}, Γ_m, s) and (3) energy release parameters $(\varepsilon_{mag}; \varepsilon_{el}, p, \zeta)$. To these one must add $(\theta_{jet}, \theta_{obs})$ if the ejecta is jet-like. In this section we asses the effect of these parameters, and consider also the situation where E_0 and Γ_0 have an anisotropic distribution in the ejecta, which, in the simplest case, introduces one more parameter representing the angular scale of such anisotropy. We compare our numerical results to the observed X-ray (2–10 keV), optical (V magnitude) and radio (4.9 GHz) afterglows. We will be looking in particular for the parameter values that yield X-ray and/or optical light-curves similar to GRB 970508, for which a fairly uniform time coverage is available.

4.1. Spherically Symmetric Ejecta

The simplest case is that of spherically symmetric ejecta with a single impulsive input of energy. Under the simplifying assumptions of a relativistic and adiabatic remnant, the equations (20) – (23) predict the asymptotic radio, optical and X-ray afterglow. For the range of times considered here, ν_p is below optical frequencies and only the radio emission shows a peak. This peak generally occurs before ν_p reaches few GHz, and it is due to the remnant's transition from the relativistic to the non-relativistic regime. For a homogeneous external medium ($\alpha = 0$), radiative electrons and $p = 2.5$, the above-mentioned equations for

a relativistic remnant yield for $\nu > \nu_p$ (optical and X-ray fluxes)

$$F_{O,X} \propto \varepsilon_{mag}^{1/8} \varepsilon_{el}^{3/2} \zeta^{-1/2} E_0^{9/8} T^{-11/8}, \quad (28)$$

while radio flux F_R is given by equation (20). If electrons are adiabatic, then

$$F_{O,X} \propto \varepsilon_{mag}^{7/8} \varepsilon_{el}^{3/2} \zeta^{-1/2} E_0^{11/8} n_d^{1/2} T^{-9/8}, \quad (29)$$

$$F_R \propto \varepsilon_{mag}^{1/3} \varepsilon_{el}^{-2/3} \zeta^{5/3} E_0^{5/6} n_d^{1/2} T^{1/2}. \quad (30)$$

These analytical approximations are consistent, within their range of validity, with the numerical results shown in Figure 1. For all the the afterglows shown in Figure 1, the γ_m -electrons become adiabatic for T between 0.01 and 10 days, while the remnant enters the non-relativistic phase at times between 10 and 300 days, when a slow but steady steepening of the light-curves can be seen. Figure 1 also shows (with symbols) observational data taken from IAU Circulars, van Paradijs et al. (1997), Sahu et al. (1997), Frail (1997), Piro et al. (1998) or inferred from the data presented by Galama et al. (1997), Bartolini et al. (1998), and Sokolov et al. (1998). The numerical results are not meant to be fits to the observational data.

If the optical and X-ray electrons are radiative, the afterglows arising from fireballs with larger initial energy or energy release parameters are brighter, as implied by equation (28). Fireballs with harder electron distributions lead to afterglows that have a shallower temporal decay (Figure 1[a2]), as predicted by equations (21) and (23). If the electron injection fraction ζ is sufficiently small, the radio afterglow can be undetectable (see eq. [30]). The peak of the radio light-curve for the $\zeta = 10^{-2}$ afterglow shown in Figure 1 is $\sim 10 \mu\text{Jy}$. For the same afterglow the synchrotron peak from γ_m -electrons remains above the optical range for several days, leading to an optical afterglow that is flat for the same duration (see Figure 1[a2]). The non-detection of radio emission from a remnant that yields observable optical afterglows could also be due to an inhomogeneous external medium: the peak of the radio emission of the $\alpha = 2$ (pre-ejected wind) case shown in Figure 1 is $\sim 30 \mu\text{Jy}$.

There are some important differences between the light-curves arising from a fireball running into a homogeneous external medium and into a pre-ejected wind. First note that Figure 1(b1) shows that when the electrons emitting at fixed frequency (here, in X-ray) are radiative, the afterglow is indeed independent of the external medium parameters n_d and α (if $\alpha \leq 1$), as predicted by equation (21). The optical and the radio afterglows depend on α (this is also true for the X-ray light-curve if $\alpha > 1$), indicating that in these cases the electrons that radiate most of the light in the corresponding energy bands are adiabatic (eqs. [22] and [23]). In a relativistic remnant, the lab-frame synchrotron cooling timescale $t_{sy} \propto \Gamma/(\gamma_e B^2)$ for electrons radiating at a peak frequency $\nu_p(\gamma_e) \propto \gamma_e^2 B \Gamma > \nu_p(\gamma_m)$ equal to a fixed observing frequency ν is $t_{sy} \propto \nu^{-1/2} (\Gamma/B)^{3/2}$, leading to:

$$t_{sy} \propto \varepsilon_{mag}^{-3/4} \Gamma_0^{\alpha/2} E_0^{-\alpha/4} n_d^{-(3-\alpha)/4} \nu^{-1/2} t^{3\alpha/4}. \quad (31)$$

which is constant in time for a homogeneous external medium, and increases as $t^{3/2}$ for a pre-ejected wind. The adiabatic cooling timescale increases as t , if the comoving density tracks the post-shock density. Therefore the electrons radiating above ν_p (i.e. in optical and X-ray) that are radiative, remain so during the entire afterglow if the external medium is homogeneous but eventually become adiabatic if the fireball interacts with a pre-ejected wind. The radiative regime of the electrons that emit at a given frequency changes with the index of the external medium, as implied by the increase of t_{sy} with α (eq. [31]), and as suggested by the light-curves shown in Figure 1(b1) and 1(b2): for $\alpha = 0$ the X-ray and optical electrons are radiative, for $\alpha = 1$ only the electrons emitting in X-ray are radiative, while for $\alpha = 2$ they are all adiabatic. Another

important difference between the homogeneous and pre-ejected external media models is manifested by the duration of the relativistic phase. From equation (19) one can calculate the dependence on model parameters of the time T_{nr} when the remnant becomes non-relativistic ($\Gamma \lesssim 2$):

$$T_{nr} \propto (E_0/n_d)^{1/3} \Gamma_0^{2\alpha/(9-3\alpha)}. \quad (32)$$

Obviously, T_{nr} is Γ_0 -independent for $\alpha = 0$, but it depends strongly on the fireball initial Lorentz factor in the case of a pre-ejected wind: $T_{nr} \propto \Gamma_0^{4/3}$, implying that in this case the relativistic phase lasts $\gtrsim 100 \Gamma_{0,2}^{4/3}$ times longer than in the homogeneous external medium case. The optical brightness of the $\alpha = 2$ afterglow is correspondingly weaker, as shown in Figure 1(b2).

We have ignored the effects of low-frequency synchrotron self-absorption in the radio range, therefore the Figures 1(a3) and 1(b3) give essentially an upper limit to the optically thin radio flux expected in this case. A simple analytical derivation of the absorption frequency is straightforward (Mészáros & Rees 1997), but it can easily lead to misleading results, since the fireball contains electrons with random Lorentz factors that span more than one order of magnitude, all emitting and absorbing the synchrotron radiation. Taking into account only the newly shocked electrons and ignoring a possible low-energy tail of the electron distribution below γ_m , it can be shown (Panaiteescu & Mészáros 1998) that the self-absorption frequency is $\nu_{ab} \sim 6.4 (10 \varepsilon_{mag})^{1/5} (10 \varepsilon_{el})^{-1} n_0^{3/5} E_{0,52}^{1/5} T^0$ GHz (at redshift $z = 1$) for a relativistic remnant and adiabatic electrons, where $E_{0,52} = E_0/(10^{52} \text{ ergs})$ and $n_0 = n_d/(1 \text{ cm}^{-3})$. This result is valid until the remnant becomes non-relativistic or until the shocked material escape sideways, if the remnant is a jet. Therefore the optical thickness is $\tau = 1.6$ at 4.9 GHz for $\varepsilon_{el} = \varepsilon_{mag} = 0.1$, $n_0 = 1$ and $E_{0,52} = 1$, indicating that the radio fluxes shown in Figures 1(a3) and 1(b3) are overestimated by a factor of $\tau(1 - e^{-\tau})^{-1} \sim 2$. Post-shock mild re-acceleration of the cooling electrons or an electron (acceleration) injection fraction ζ below unity can further decrease the radio flux by reducing the number of the low energy electrons in the remnant.

In its simplest form considered in Figure 1, the fireball shock model obviously cannot explain departures from the power-law decay, such as observed in the optical afterglow of GRB 970508 near $T \sim 2$ days. A brightening of the afterglow may arise if there is a delayed energy input, as illustrated in Figure 2. The energy injection index s was set equal to a large value so that the input resembles a second relativistic shell that catches up with the initial fireball. For a delayed energy input E_{inj} comparable to or larger than the energy of the remnant E_0 , the light-curves exhibit a bump at the time of interaction between the two shells. The larger E_{inj} is, the more prominent is the resulting bump. For lower Γ_m , the collision takes place later, and this might explain a secondary departure from a power-law, apparent in the optical afterglow of GRB 970508 at $T \gtrsim 50$ days. (the flattening of the light-curve could also be due to a constant contribution of the host galaxy – Pedersen et al. 1998).

In Figure 2, the minimum Lorentz factor Γ_m was chosen such that the numerical light-curve exhibits the brightening observed in the 970508 optical afterglow after $T = 1$ day. All light-curves shown in Figure 2 were calculated using the same fireball initial energy $E_0 = 6 \times 10^{51}$ ergs, delayed energy injection (from refreshed shocks) $E_{inj} = 3 E_0$ (yielding a total energy $E_0 + E_{inj} = 2.4 \times 10^{52}$ ergs), and $\Gamma_m = 11$, and the same set of parameters $(n_0, \alpha; \varepsilon_{mag}; \varepsilon_{el})$. The model shown with dotted lines corresponds to constant parameters p and ζ , chosen such that the slope of the late optical power-law decay and the early time radio fluxes are close to the observed ones. The corresponding X-ray afterglow is too faint, while the early optical and late radio afterglows are too bright. Generally, such discrepancies cannot be resolved by adjusting the dynamical parameters $(E_0, E_{inj}, \Gamma_m; n_0, \alpha)$ or the energy release parameters $(\varepsilon_{mag}; \varepsilon_{el})$, as changes in these parameters alter the multi-wavelength light-curves in a similar fashion. However, a physically plausible possibility is that changes occur in the parameters p and ζ which determine the shape of the synchrotron spectrum, and these can alter the light-curve in a given band without significant changes in other bands.

For times $T \gtrsim 0.3$ days in Figures 1 and 2, the synchrotron peak ν_p is below the optical band, so that the relative intensity of the optical and the X-ray fluxes is determined only by the slope of the spectrum above ν_p . This suggests that a brighter X-ray afterglow and a dimmer optical light-curve can be obtained by using a flatter electron index p , as illustrated by the early X-ray and optical fluxes shown with dashed lines in Figure 2. If p were held constant at 1.4 during the entire afterglow, the resulting optical light-curve would decay much slower than for $p = 2.3$ (see eq. [21]), and thus would be clearly inconsistent with the observational data. A better simultaneous fit of the X-ray and optical afterglows can be obtained if one assumes that the electron index changes during the evolution of the remnant. In the model shown with dashed lines in Figure 2, we considered that the index $p = 1.4$ is constant until the second shell of ejecta catches up with the fireball ($T \sim 2$ days), and changes to $p = 2.3$ at the end of the collision between the two shells. The indices p before and after the delayed energy input were chosen so that the numerical result fits the early X-ray to optical emission ratio and the decay of the observed optical light-curve. The electrons that radiate most of the V -band light shown in Figure 2 are radiative, with some smaller contribution from the adiabatic γ_m -electrons, implying that the optical spectrum should have a slope close to $-p/2$. The change from $p = 1.4$ to $p = 2.3$ at $T \sim 2$ days is consistent with the optical spectral slopes reported by Djorgovski et al. (1997) (-0.65 ± 0.30 at $T \sim 1$ day), Metzger et al. (1997) (-0.9 ± 0.3 at $T \sim 2$ days), and Sokolov et al. (1998) (-1.1 for T between 2 and 5 days).

The radio afterglow at times shown in Figure 2 ($T > 3$ days) depends on the late value of index p . Unlike the emission at optical and X-ray energies, the emission at radio frequencies is due to all the electrons in the remnant, whether they are the first accelerated electrons (that have cooled and emit only in radio) or the more energetic, recently accelerated electrons (that radiate at higher frequencies but extend their emission down into radio through the low energy synchrotron tail of slope 1/3). The later electrons slightly dominate the radio emission after $T \sim 10$ days, and lead to the large fluxes shown with dotted line ($\zeta = 0.2$) in Figure 2. This contribution to the radio emission is diminished if the recently accelerated electrons have a higher post-shock acceleration Lorentz factor, which can be achieved if the electron injection fraction ζ is decreased (see eq. [10]). This is shown by the dot-dashed line in Figure 2, where it was assumed that the electron acceleration injection fraction drops from $\zeta = 0.2$ to $\zeta = 0.05$ when the remnant approaches the non-relativistic regime ($\Gamma \sim 3$). At the same time the optical afterglow exhibits a brightening due to the fact that for $\zeta = 0.05$ the synchrotron peak ν_p is closer to the optical range.

4.2. Axially Symmetric Jets

Jet-like outflows obviously reduce the energy requirements of fireballs, which, if extending over 4π sr, would require a total energy above 10^{52} ergs to produce the optical fluxes observed in the afterglow of GRB 970508. In Figure 3(a) we show light-curves arising from jet ejecta whose properties are isotropic within the opening angle θ_{jet} . From these numerical results, we can draw several conclusions:

(1) As expected, the light-curve decay steepens when the observer sees the edge of the jet. This is shown by the departure of the dotted line (jet, observer located on the jet axis) from the thick solid line (isotropic fireball) around $T = 6$ days. The smaller θ_{jet} , the earlier such a steepening occurs.

(2) Jets seen at angle $\theta_{obs} < \theta_{jet}$ do not exhibit the rise shown by jets with $\theta_{obs} > \theta_{jet}$.

(3) The larger θ_{obs} , the more delayed and dimmer the afterglow peak. For energies $E_0 \lesssim 10^{51}$ ergs, the optical emission from jets located at $z = 1$ that are seen at an angle $\theta_{obs} > 2\theta_{jet}$, is unlikely to be detected. The afterglow that fits best the observations is obtained when energy injection is included. The thin solid line in Figure 3(a) is for a total delayed energy input 4 times larger than the initial energy of the jet, leading

to a total available energy of 1.9×10^{51} ergs.

In a more realistic scenario, the explosive event that generates the ejecta may lead to an angle-dependent energy distribution, as considered by Mészáros et al. (1998). Figure 3(b) (which is not meant as a fit to the afterglow of GRB 970508), shows the effect of such an anisotropic distribution for the particular choice where the energy per unit solid angle in the jet is an exponential in the polar angle θ : $(dE_0/d\Omega)(\theta) = (dE_0/d\Omega)_{axis} \exp(-\theta/\theta_E)$. For $\theta_E > 0$ the angular energy density decreases toward the jet edge while for $\theta_E < 0$ it increases. The same angular dependence (with the same angular scale θ_E) was assumed for Γ_0 . The initial Lorentz factor has no effect on the light-curve if the external medium is homogeneous, as shown in the previous section; the motivation for this choice was simply an isotropic mass distribution in the ejecta. To maximize the effect of the anisotropy in the ejecta, the observer was placed on the jet axis, and a large jet opening was chosen in order to separate this effect from the “edge effect”. In all cases, the energy density at $\theta = 0^\circ$ was set to $10^{52}/\pi$ ergs/sr, which leads to the following total jet energies: $E_{0,52} = 1$ for the isotropic distribution ($\theta_E = \infty$), $E_{0,52} = 0.2$ for $\theta_E = \theta_{jet}/3$ and $E_{0,52} = 8.6$ for $\theta_E = -\theta_{jet}/3$. The light-curve decays agree qualitatively with the results of Mészáros et al. (1998): if $dE_0/d\Omega > 0$, then more energy is emitted from fluid moving at larger angles relative to the LSC, arriving later at detector, and yielding shallower decays than in the isotropic case. Conversely, if $dE_0/d\Omega < 0$, then most energy is radiated away by the fluid moving close to the LSC; this radiation arrives earlier at the detector and leads to steeper light-curve decays.

The case where the observer is located off the jet axis is considered in Figure 3(c). The parameters $(dE_0/d\theta)_{axis}$ and θ_E were chosen so that the total energy of the jet is the same in all cases. The conclusion that can be drawn from Figure 3(c) is that, for all other parameters fixed, the light-curve seen by an off-axis observer is determined mainly by the total energy of the jet and not by how this energy is distributed. The ironing out of the details of the angular energy distribution in an axially symmetric jet is due to the differential relativistic beaming of the radiation emitted by fluid moving at angles between $\theta_{obs} - \theta_{jet}$ and $\theta_{obs} + \theta_{jet}$ relative to the LSC.

Jets with the parameters given for Figure 3(a) and 3(c) can explain the rise and decay of the light-curve of GRB 970508 after $T \sim 0.5$ days. The emission detected in the early part ($T \lesssim 0.5$ day) of the optical afterglow may be due to some ejected material lying outside the main jet. In Figures 3(a) and 3(c) we show with dot-dashes lines the emission from such a large angle outflow, containing $E_0 = 7.0 \times 10^{50}$ ergs, ejected isotropically outside of the central jet of opening angle $\theta_{jet} = 10^\circ$, whose axis of symmetry is offset by $\theta_{obs} = 14^\circ$ relative to the LSC. The sum of the light-curves from such a two-component ejecta (central jet and large angle outflow) matches well the features observed in the afterglow of GRB 970508. The X-ray afterglow can be fitted as before together with the optical, by making an appropriate choice of the electron index p in the jet and in the large angle outflow.

5. Conclusions

Previous models of GRB afterglow light-curves from cosmological fireball shocks (e.g. Mészáros et al. 1998; Rees & Mészáros 1998; Sari, Piran & Narayan 1998) have used analytical descriptions based on scaling laws valid in the asymptotic limits. These require simplifying assumptions and involve various undetermined parameters. The most important analytical results on the afterglow light-curve are given in section §3. They should be used with care when making comparisons with observed power-law decays, as electrons with different random Lorentz factors can be in different radiating regimes. Generally, those elec-

trons radiating in optical and X-ray are radiative, while those radiating at radio frequencies are adiabatic, at least as long as the remnant is relativistic. Moreover, the analytical light-curves do not take into account the shape of the equal-arrival time surface, and assume that there is a one-to-one correspondence between the lab-frame time of emission and the detector time.

Numerical calculations provide the environment where the assumptions made in analytical derivations can be tested and relaxed, and where results are expected to be more accurate. In some cases, like that of a fireball in a mildly relativistic regime, or like that of jet ejecta seen at an angle $\theta_{obs} \neq 0^\circ$, it is cumbersome to obtain analytical results. At the level of numerical calculations, effects arising from the viewing geometry (the equal arrival time surface is not the same as the equal lab-frame time surface) or from details of the energy release (e.g. an accurate tracking of the evolution of the electron random Lorentz factor γ_e) can be properly accounted for.

We have solved the differential equations for the afterglow evolution and integrated the remnant emission to calculate light-curves with different model parameters. Energy injection (refreshed shocks), angular anisotropy and jet-like structure of the ejecta allow for a variety of possible behaviors of the numerical light-curves, even under the assumption of axial symmetry in the remnant. More than one scenario could explain a fairly large fraction of the optical data of the GRB 970508 afterglow. A spherically symmetric ejecta with energy injection up to a total energy of 2.4×10^{52} ergs, or a jet of opening 10° seen at an angle of 14° , in which energy is injected up to a total of $\sim 2 \times 10^{51}$ ergs, both located at redshift $z = 1$, seem to fit most the mentioned afterglow. Such energies are quite conservative in a cosmological scenario, and clearly do not require any drastic departures from the simple fireball/firejet scenario. Using a variable index of the electron power-law distribution, we obtained a simultaneous good fit of the X-ray and optical afterglow of GRB 970508. Synchrotron self-absorption, post-shock re-energization of the electrons or a decrease in the electron acceleration fraction reduce the radio fluxes obtained numerically and yield a better fit of the radio data, but this comparison is much more uncertain and model-dependent.

The first generation of fireball shock models of afterglows were characterized by great simplicity and have predicted power-law decaying light-curves. As one would expect, relaxing some of the assumptions that are usually made in the simplest versions of these models, such as isotropy of the ejecta or constancy of the parameters that quantify the energy release, leads to an improved agreement between numerical results and observations. All of the models presented here still contain simplifying assumptions (e.g. axial symmetry, power-law delayed energy input), which were taken as a starting point in investigating the features of the numerical light-curves. While the present data do not require it, relaxing these assumptions could lead to even more diverse afterglow light-curves. The variety of behavior exemplified by the models we have discussed highlights the potential importance of afterglow data as diagnostics for the dynamics and anisotropy of the ejecta, and emphasizes how much more can be learned when the sample has grown larger.

We are grateful to NASA NAG5-2857, NAG 3801 and the Royal Society for support, and to R.A.M.J. Wijers and D. Reichart for useful comments.

REFERENCES

Bartolini, C., Beskin, G., Guarneri, A., Masetti, N. & Piccioni, A. 1998, in *Gamma-Ray Bursts, Fourth Huntsville GRB Symposium*, eds. C. Meegan, R. Preece, & T. Koshut (New York:AIP), in press (astro-ph/9710313)

Blandford, R. D. & McKee, C. F. 1976, *Phys. Fluids*, 19, 1130

Djorgovski, S. G. et al. 1997, *Nature*, 387, 876

Frail, D. et al. 1997, *Nature*, 389, 261

Galama, T. et al. 1997, *Nature*, 387, 479

Garcia, M. R. et al. 1998, *ApJL*, accepted (astro-ph/9710346)

Mészáros , P. & Rees, M. J., 1997, *ApJ*, 476, 232

Mészáros , P., Rees, M. J., & Wijers, R. 1998, *ApJ*, 499, 301

Metzger, M. R. et al. 1997, *Nature*, 387, 878

Panaitescu, A. & Mészáros , P. 1997, *ApJ*, 492, 683

Panaitescu, A. & Mészáros , P. 1998, *ApJ*, 501, in press (astro-ph/9711339)

van Paradijs, J. et al. 1997, *Nature*, 386, 686

Pedersen, H. et al. 1998, *ApJ*, 496, 311

Piro, L. et al. 1998, *A&A*, 331, L41

Rees, M. J. & Mészáros , P. 1998, *ApJ*, 496, L1

Reichart, D. 1998, *ApJ*, 495, L99

Rhoads, J. E. 1998, *ApJ*, submitted

Sahu, K. C. et al. 1997, *Nature*, 387, 476

Sari, R., Piran, T., & Narayan, R. 1998, *ApJ*, 497, L17

Sokolov, V. V. et al. 1998, *A&A*, in press (astro-ph/9709093)

Tavani, M. 1997, *ApJ*, 483, L87

Vietri, M. 1997, *ApJ*, 488, L105

Waxman, E. 1997, *ApJ*, 485, L5

Waxman, E., Kulkarni, S. & Frail, D. 1998, *ApJ*, 497, 288

Wen, L., Panaitescu, A., & Laguna, P. 1997, *ApJ*, 486, 919

Wijers, R., Rees, M. J. & Mészáros , P. 1997, *MNRAS*, 288, L51

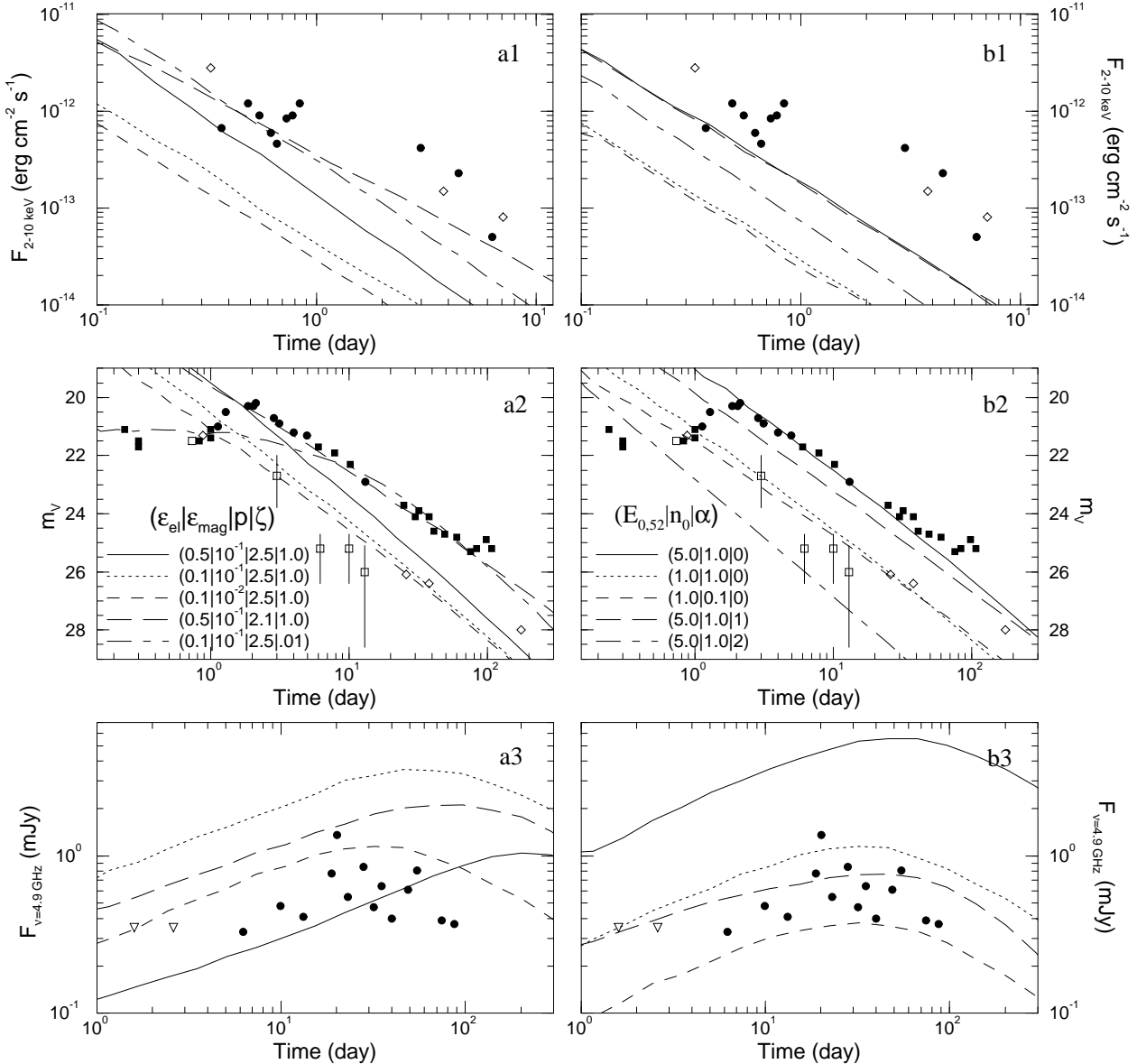


Fig. 1.— The effect of the energy release (left graphs) and dynamical (right graphs) parameters on the light-curve from a simple spherically symmetric fireball, without refreshed shocks. Legends give the parameters for each case. For each curve there is another one that differs in only one parameter, allowing assessment of its effect. Other parameters are: $E_{0,52} = 1$, $n_0 = 1$, $\alpha = 0$ for graphs (a1)–(a3), and $\varepsilon_{mag} = 10^{-2}$, $\varepsilon_{el} = 0.1$, $p = 2.5$, $\zeta = 1$ for graphs (b1)–(b3). Observational data: open symbols are for GRB 970228, filled symbols for GRB 970508. Graphs (a2) and (b2): V magnitudes inferred from R_C magnitudes are shown as squares. Error bars are given only for magnitude errors larger than 0.5. Graphs (a3) and (b3): triangles indicate upper limits. The radio light-curves for the $\zeta = 10^{-2}$ and $\alpha = 2$ afterglows have peak fluxes of 10 μ Jy and 30 μ Jy, respectively, and do not appear in graphs (a3) and (b3). A redshift $z = 1$ in a $H_0 = 75 \text{ km s}^{-1} \text{Mpc}^{-1}$, $\Omega = 1$ Universe is assumed. The radio fluxes plotted are the optically thin upper limits; the inclusion of synchrotron self-absorption and/or electron re-energization would lead to lower radio fluxes (§4).

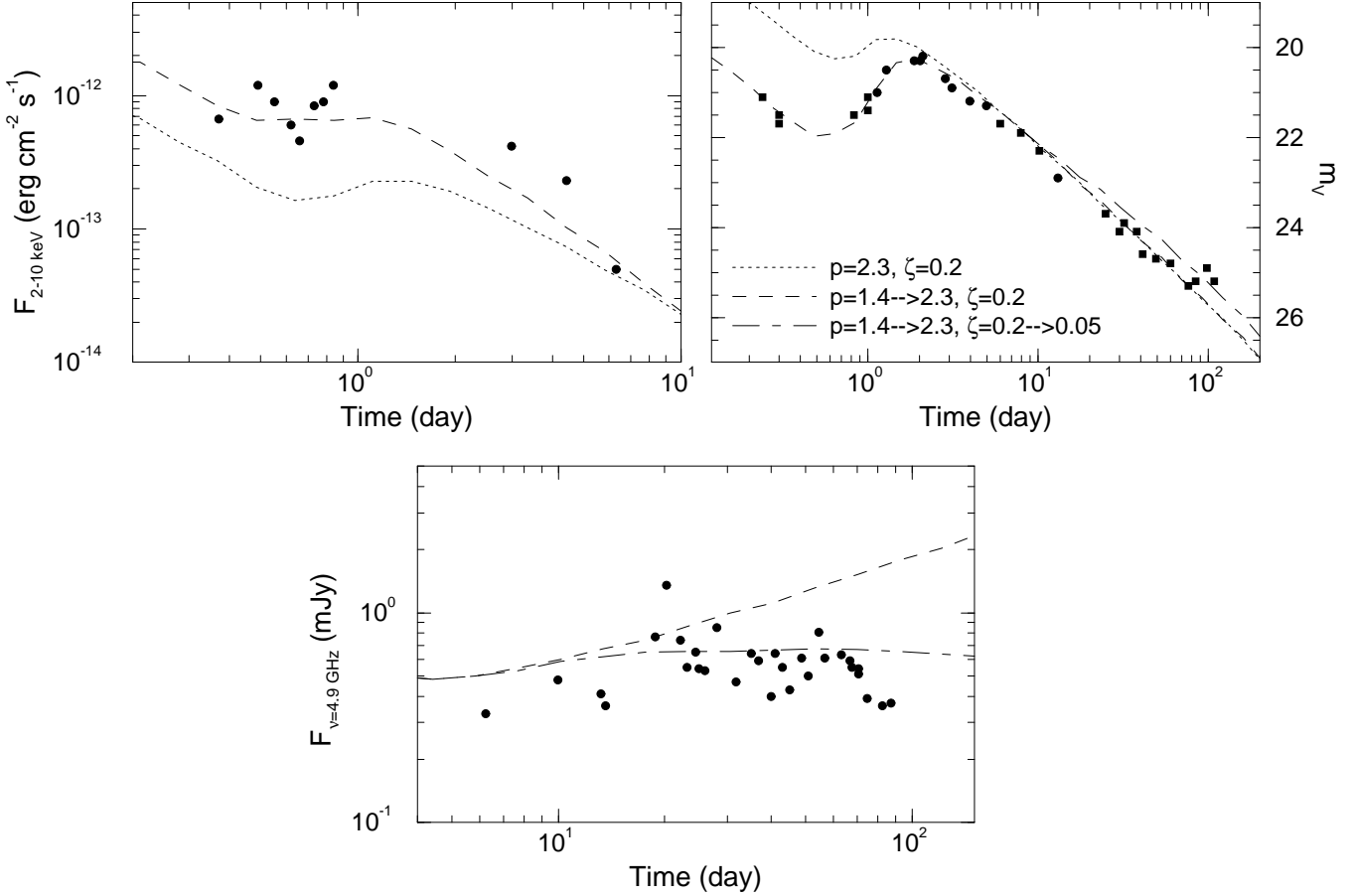


Fig. 2.— Effect of refreshed shocks in an isotropic fireball, caused by a late energy input which is a power law in the Lorentz factor Γ_f of the ejecta that catches up with the fireball (§2.2). All models have the same initial and injected energies $E_{0,52} = 0.6$, $E_{inj} = 3 E_0$, as well as the same minimum Lorentz factor of the delayed energy input $\Gamma_m = 11$. The injection index s has a large value, leading to an impulsive energy input at Γ_m and to a distinctive step-like brightening of the afterglow. Other parameters are: $\varepsilon_{mag} = 0.1$, $\varepsilon_{el} = 0.1$, $n_0 = 1$, $\alpha = 0$, $z = 1$. An absorption of $A_V = 0.25$ mag (Reichart 1998) at the source redshift was assumed. The electron index p and acceleration fraction ζ for each model are given in the legend of the optical light-curves. They are constant for the model shown with dotted lines, p changes at the end of the delayed energy input for the dashed and dot-dashed lines models, while ζ decreases when the remnant ends the relativistic expansion only for the model shown with a dot-dashed line. Symbols represent the data for the GRB 970508 afterglow.

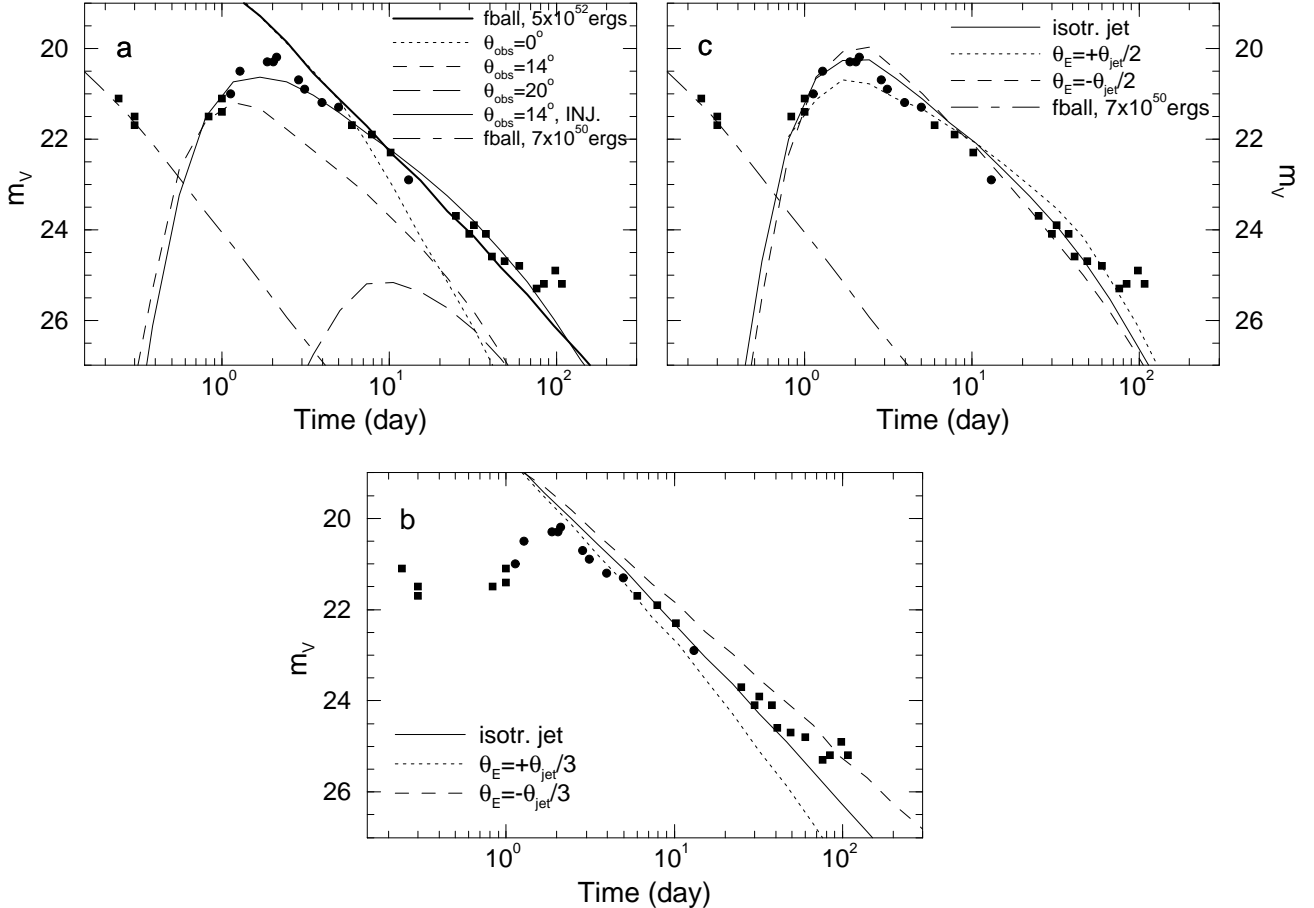


Fig. 3.— Optical light-curves from jet-like ejecta, compared to data points for GRB 970508. (a) An outflow which is isotropic within a jet of opening half-angle $\theta_{jet} = 10^\circ$, seen at the different angles θ_{obs} , for $E_0 = 3.8 \times 10^{50}$ ergs, $n_0 = 1$, $\alpha = 0$, $\varepsilon_{mag} = 0.1$, $\varepsilon_{el} = 0.1$, $p = 2.5$, $\zeta = 1$, $z = 1$. For comparison, the afterglow from a spherically symmetric remnant with the same parameters, except $E_0 = 5 \times 10^{52}$ ergs (yielding the same energy density per solid angle), is also shown (solid thick line). A numerical light-curve matching the observational data (solid thin line) corresponds to $\theta_{obs} = 14^\circ$ and energy injection characterized by $E_{inj} = 1.5 \times 10^{51}$ ergs, $\Gamma_m = 2$ and $s = 1.5$. (b) Effect of an anisotropic angular distribution of energy inside a jet with $\theta_{jet} = 60^\circ$, $\theta_{obs} = 0^\circ$, $(dE_0/d\Omega)_{axis} = 10^{52}/\pi$ ergs/sr. Other parameters ($n_0, \alpha; \varepsilon_{mag}, \varepsilon_{el}, p$) are the same as for graph (a). The legend gives the angular scale θ_E (see text). (c) The same jet as in (a) seen at $\theta_{obs} = 14^\circ$, but with different energy per solid angle distributions. All jets have the same energy $E_0 = 1.5 \times 10^{51}$ ergs, isotropically distributed (solid line), exponentially decreasing toward the jet edge (dotted line) or exponentially increasing toward the edge (dashed line). Also shown in graphs (a) and (c) with dot-dashed lines is the contribution from an ejecta which is isotropic everywhere outside of the jet with opening angle $\theta_{jet} = 10^\circ$ and orientation $\theta_{obs} = 14^\circ$. The isotropic component has an energy 7×10^{50} ergs (other parameters are as for [a]) and can account for the early ($T \lesssim 1$ day) afterglow emission.